Quantitative Characterization of Mitral Annulus and Leaflets from Transesophageal 3D Echocardiography

Miguel Sotaquirá[1], Laura Fusini[2], Mauro Pepi[2], Roberto M Lang[3], Enrico Caiani[1]

[1]Dipartimento di Elettronica, Informazione e Bioingegneria, Politecnico di Milano, Milan, Italy
[2]Centro Cardiologico Monzino IRCCS, Milan, Italy
[3]Noninvasive Cardiac Imaging Laboratory, University of Chicago, Chicago, IL, USA

Abstract

We propose and validate a novel algorithm for the segmentation and quantification of the mitral annulus (MA) and mitral leaflets (ML) from transesophageal real-time 3D echocardiography volumes in a closed mitral valve (MV) configuration. Following initialization of 8 MA points and of the coaptation line, the MA and the anterior and posterior ML are automatically obtained in 3D. Once segmented, several morphological parameters, including local ML thickness and tenting, are obtained. Validation versus manual tracings was performed in 33 patients: 9 controls, with normal MA dimensions, 12 patients with dilative cardiomyopathy and 12 after MV repair with insertion of annuloplasty ring on the posterior MA region. MA and ML segmentations showed a high level of accuracy when compared with manual tracings, with errors of the order of the voxel size. Computed parameters were comparable with those found in literature for healthy MV. The potential clinical applicability to different MV pathologies, as well as repaired valves with implanted annular rings, was favorably tested.

1. Introduction

The mitral valve (MV) allows the flowing of blood from the left atrium (LA) into the left ventricle (LV) during diastole, and prevents it during LV systole. One of its anatomic components is the mitral annulus (MA), a three-dimensional (3D) saddle shape ring, to which the anterior (A) and posterior (P) mitral leaflets (ML) are attached. Recently, transesophageal real-time 3D echocardiography (RT3D TEE) has enabled accurate morphologic and quantitative assessment of the MV apparatus, but despite its extended use morphological quantification of MA and ML datasets remains a challenge, and commonly it is performed using strategies that rely on manual and time-consuming segmentation procedures[1].

Several semi-automatic approaches aimed at segmenting the MA and ML have been developed [2-4]. Despite being able to correctly segment the MA, they make use of geometrical, morphological or mechanical priors to infer the closed valve ML configuration, constraints that are not patient-specific and can therefore not be fully verified in presence of MV pathologies. In addition, none of the proposed methods fully computes and exploits the local morphology of ML thickness and tenting, thus limiting the clinical applicability of those approaches.

Our aims were: 1) to develop a novel semi-automated approach requiring minimal user interaction and reducing the number of constraints, for the segmentation of MA and ML from RT3D TEE datasets in the closed MV configuration (systolic phase), also capable of computing novel parameters such as regional leaflet thickness and tenting; 2) to validate it by comparison with a "gold standard" manual tracing in patients with different pathologies. The algorithm was tested on a set of 33 patients including normal and diseased valves, and comparisons with a gold standard were made for each volume in the dataset.

2. Methods

2.1. Population and imaging protocol

Subjects were enrolled at Centro Cardiologico Monzino (Milan, Italy) and at the University of Chicago Hospitals (Chicago, IL). The protocol was approved by the respective institutional review boards, and informed consent was obtained in all participants.

Inclusion criteria were: 1) patients with DCM (ejection fraction < 35%) undergoing a clinically indicated TEE examination; 2) patients with degenerative MV disease and severe MR (effective regurgitant orifice area $\geq 0.4 cm^2$ estimated by proximal isovelocity surface area technique or with a vena contracta width >7 mm) undergoing intra-operative TEE during MV repair with implantation of U-shaped annular rings (Cosgrove-Edwards© rings).

As a result, 12 patients with dilative cardiomyopathy

(DCM) (5 Female, 7 male, 70±9 years), and 12 patients undergoing MV repair with annuloplasty ring insertion (MVR) (2 Female, 10 male, 62±14 years) were studied. In addition, a control group (NL) of 14 patients (14 males, 50±10 years) undergoing TEE to rule out a cardioembolic source with normal LV function were studied. Exclusion criteria were (1) associated MV stenosis, (2) tricuspid regurgitation greater than mild, (3) aortic valve disease, (4) contraindications to TEE, (5) atrial fibrillation and cardiac arrhythmias, (6) myocarditis or pericardial or congenital heart disease, and (7) more than mild MR.

Each dataset was acquired using the using the iE33 system (Philips Medical Systems, Andover, MA) and then converted to Cartesian from the original frustum coordinates system, with dimensions of roughly 200x200x200 voxels with a resolution ranging from 0.2 to 1.0 mm.

2.2. MA and ML morphology

Datasets were analyzed using custom software [5]. Briefly, the frame preceding aortic valve closure in the RT3D TEE dataset was selected for analysis; then, two couples of opposite reference annular points (anterior, A; posterior, P; anterolateral, Al; posteromedial, Pm) on two orthogonal cut-planes, and four additional points symmetrically positioned around A on evenly-rotated (30º apart) cut-planes, were selected (Figure 1, a); in addition one point located on the LA was selected to ensure that on each cut-plane the LA lie on top of the MV. From this set of points, both the MA 3D contour (Figure 1, a) and the ML surface were automatically detected using a conventional block-matching algorithm, combined with morphological operations and a graph-based procedure[5]. In addition to conventional global parameters, a set of novel parameters describing the local morphology of the ML was computed:

(1) Regional thickness: computed as twice the value of the distance transform through the leaflets medial-axis on each cut-plane.

(2) Regional tenting height: defined as the vertex-to-vertex distance between the MA and ML meshes, both sharing the same *x*, *y* coordinates and differing only by the *z* coordinate.

From the detected ML surface visualized in volume rendering using a color map representing the regional tenting height information, overimposed to the original RT3D volume, the coaptation line (CL) was obtained by manually selecting between 4 and 6 points (Figure 1, b), and then automatically constructing a path between consecutive pairs of the initialized points using a Dijkstra graph-based algorithm (Figure 1, c).

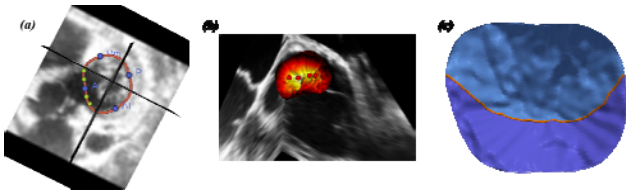

Figure 1. Overview of the MV segmentation algorithm. (a) Location of the initialization points and the segmented MA (red contour); (b) initialization of the CL detection algorithm; (c) the resulting CL (red curve) and the extracted A and P ML (light and dark 3D surfaces).

2.3. Validation protocol

MA and ML automated segmentations were compared point-to-point with manual tracings, "gold standard", performed by an expert cardiologist by computing Euclidean distances expressed in pixels in 2D space. The tracing was performed on each of the 36 radial cut-planes, resulting into the 72 points corresponding to the MA locations, and respective leaflets medial axes.

To validate the accuracy in the computation of the ML regional thickness and regional tenting height, the same set of radial cut-planes and corresponding automated and manual tracings were used. For each pair of corresponding radial cut-planes and tracings, the local 2D thickness and ML tenting were computed, and corresponding errors, in pixels, were then obtained.

To represent the average error distribution in the considered groups, the local error distribution obtained from each dataset was remapped into a circular parametric map. Then, results from the considered patients were combined to compute a parametric map of median errors for each population. In all cases, errors are presented as median, 25^{th} and 75^{th} percentiles.

3. Results

3.1. Accuracy of MA segmentation

Table 1 summarizes the errors for each group of patients, and it is evident that the algorithm offers the same level of accuracy both in normal and diseased MVs. In particular, errors of the order of 1.0 pixels (corresponding to 1.0 mm for the broadest space resolution in the studied dataset) were observed in all annular regions.

3.2. Accuracy of ML segmentation

Median errors obtained for the MA segmentation as well as for the computation of regional thickness and tenting, are listed in Table 2. As seen from this table, ML errors in segmentation and quantification of regional thickness and tenting were not population dependent, and

the errors, below the order of a pixel, were comparable among groups.

Table 1. Distribution of regional errors of the MA segmentation algorithm for each of the analyzed groups. Errors are presented as median, 25th and 75th percentiles

Group / Annular section	NL	DCM	MVR
Anterior	1.2 (1.0; 2.1)	1.3 (0.8; 1.6)	1.0 (0.8; 1.8)
Antero-lateral	0.9 (0.2; 1.8)	0.9 (0.4; 1.6)	1.1 (0.3; 1.5)
Posterior	1.0 (0.0; 2.1)	1.0 (0.2; 1.4)	1.2 (0.0; 1.8)
Postero-medial	1.0 (0.6; 1.4)	0.9 (0.0; 1.6)	0.9 (0.3; 1.2)

Table 2. Distribution of regional error for the MA segmentation and quantification algorithms, for each of the analyzed groups. Errors are presented as median, 25th and 75th percentiles

Group / Variable	NL	DCM	MVR
ML segmentation	0.7 (0.5; 0.9)	0.8 (0.6; 0.9)	0.8 (0.7; 1.1)
Thickness	-0.1 (-1.4; 1.1)	-0.1 (0.1; 0.2)	0.0 (-0.1; 1.3)
Tenting	0.1 (-1.6; 1.8)	-0.2 (-0.3; 0.3)	0.2 (-1.8; 2.1)

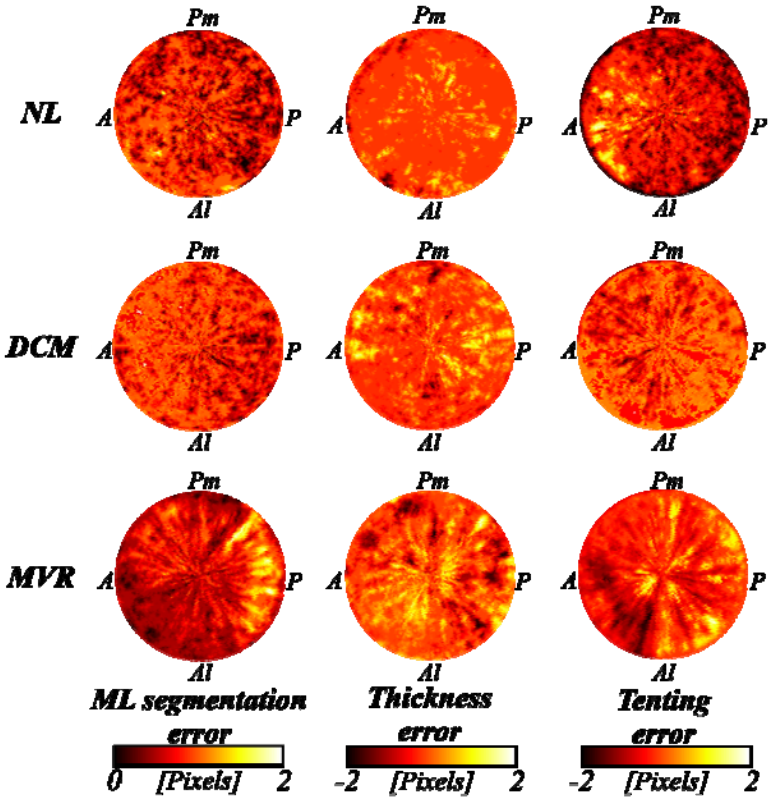

Figure 2. Parametric maps of regional error distribution for the ML segmentation and quantification algorithms. From top to bottom: NL, DCM and MVR groups; from left to right: ML segmentation error, thickness error and tenting error.

Figure 2 shows the circular parametric maps of errors for the ML segmentation (absolute errors, first column) and for thickness and tenting computation (signed errors, second and third columns respectively). The

same color scale was used for each type of error to allow visual comparison between groups.

The errors in ML segmentation were comparable among populations, and range from 0 to 2 pixels, with a median error among all groups equal to 0.8 pixels (with 25th and 75th percentiles of 0.25 and 1.2 pixels, respectively). In MVR, slightly higher errors around the posterior annular region, given the presence of suture points as a result of the annuloplasty procedure, were observed. In NL, slightly higher errors around the anterior annular portion were visible.

The median of signed errors for thickness and tenting computation show values of -0.1 pixels (-1.5; 1.2 pixels), and of 0.2 (-1.6; 1.5 pixels), respectively for these two regional parameters. Again, in NL a slightly higher tenting height overestimation, located towards the left half of the map and reflecting the positioning error shown in the ML segmentation around the anterior region, was visible. In MVR this behavior was also present, but with higher errors in thickness and tenting around the posterior annular portion, as a result of the presence of suture points mentioned previously.

Except for these local inhomogeneities, the error distribution was almost uniform around the positive and negative values, thus implying that there was not systematic bias toward under or over-estimation of the computed parameters.

4. Discussion

The proposed algorithm resulted in the quantification of MA and ML morphological parameters in approximately one fifth of the time needed by other conventional software (Philips' QLab MVQ module). Moreover, novel parameters such as local leaflet thickness and local tenting, not available in other existing (custom- based or commercial) software, were reliably quantified.

The parametric maps of median errors, used in the validation of regional thickness and tenting, allowed to evidence minimal signed errors, with local positive errors (between 1 and 2 pixels) in tenting height towards the anterior region for the NL group, probably due to the fact that these datasets were acquired with the worst spatial resolution (close to 1.0 mm), compared to the other groups, which affects the selection of initialization points in the anterior annular region. Thus, local errors in both segmentations of MA and ML affect cumulatively the tenting height computation. Also higher signed errors, both for thickness and tenting computations, were observed toward the posterior region in MVR, which can be explained by the presence of the implanted ring and in particular for the location of suture points in the ML surface.

The proposed algorithm also outperformed previous approaches [2-4] since the detection of valvular structures resulted in a more precise delineation of MA and ML: for the considered higher voxel size (1 mm), median errors of 1.1 mm (25% and 75% percentiles of 1mm and 2mm) were achieved for MA segmentation and of 0.8 mm (25% and 75% percentiles of 0.25 mm and 1.2 mm) for ML segmentation.

5. Conclusion

We proposed and validated a semi-automated algorithm for MA and ML segmentation from RT3D TEE data, capable of characterizing the global and regional morphology of the MV with minimal user interaction and no model-based constrains. Application to patients with different MV pathologies in pre and post-operative stage, with global or local leaflet thickness changes, showed the potential utility of the proposed method in the clinical setting, as well as its versatility in presence of completely different MV morphologies.

References

[1] Vergnat M, Jassar AS, Jackson BM, Ryan LP, Eperjesi TJ, Pouch AM, et al. Ischemic mitral regurgitation: a quantitative three-dimensional echocardiographic analysis. The Annals of Thoracic Surgery. 2011;91(1):157–64.

[2] Burlina P, Sprouse C, DeMenthon D, Jorstad A, Juang R, Contijoch F, et al. Patient-specific modeling and analysis of the mitral valve using 3D-TEE. Information Processing in Computer-Assisted Interventions 2010;135–46.

[3] Voigt I, Ionasec RI, Georgescu B, Houle H, Huber M, Hornegger J, et al. Model-driven physiological assessment of the mitral valve from 4D TEE. Samei E, Pluim JPW, Karssemeijer N, Miga MI, Sahiner B, Siddiqui KM, et al., editors. SPIE Medical Imaging. SPIE; 2009: 72610R1–72610R11.

[4] Mansi T, Voigt I, Mengue E, Ionasec R. Towards patient-specific finite-element simulation of MitralClip procedure. Proceedings MICCAI 2011; 452-9

[5] Sotaquira M, Fusini L, Lang RM, Caiani EG. Nearly-Automated Quantification of Mitral Annulus and Leaflets Morphology from Transesophageal Real-Time 3D Echocardiography. Computing in Cardiology 2012; 39:145–8.

Address for correspondence.

Enrico G Caiani, PhD
Dipartimento di Elettronica, Informazione e Bioingegneria,
Politecnico di Milano; P.zza L. da Vinci 32, 20133
Milan, Italy
enrico.caiani@polimi.it